Detached Plasma Studies in GOL-NB with Extra Gas Injection

**V. V. Postupaev[a],*, V. I. Batkin[a], I. A. Ivanov[a], K. N. Kuklin[a], N. A. Melnikov[a],
K. I. Mekler[a], A. F. Rovenskikh[a], and E. N. Sidorov[a]**

[a]*Budker Institute of Nuclear Physics, Siberian Branch, Russian Academy of Sciences, Novosibirsk, 630090 Russia*
*e-mail: V.V.Postupaev@inp.nsk.su

Abstract—The magnetic system of an open trap usually includes expansion sections located between high-field magnetic mirrors and end surfaces that receive plasma. In the GOL-NB device, an arc plasma gun is located in one of the expanders, which creates a low-temperature starting plasma in the confinement area. The parameters of the surface plasma sheath affect the electrical connection of the confinement area with the walls and, thereby, affect the contribution of the line-tying effect to the plasma stability and the longitudinal energy losses from the trap. The experiments with additional hydrogen injection into the plasma gun were carried out at GOL-NB. We observed a radiating plasma formation detached from the surface, which visually corresponds to that in radiating divertors in tokamaks. In both standard and detached modes, decaying plasma existed near the receiving electrodes during the entire observation time after the discharge current was terminated. In the central trap of GOL-NB, some structures in the Fourier spectrogram of magnetic fluctuations manifest earlier in the detachment mode than in the standard mode and have lower frequencies. We associate these structures with the onset of interchange-like modes due to the loss of plasma stabilization by the line-tying to the conducting ends. The observed plasma response to the additional gas supply confirmed our understanding of the line-tying effect as the main factor stabilizing the plasma core in the initial phase of density accumulation in the central trap.

Keywords: plasma detachment, divertor, linear device, multiple-mirror trap, GOL-NB

**DOI:** 10.1134/S1063780X23601967

1. INTRODUCTION

Studies of detached plasma properties are important parts of research programs in many fusion-related experimental devices (see, e.g., the review [1] and recent papers [2–14]). In this text, we will use the definition of "detached plasma" [15] as "the state in which large gradients in total plasma pressure (static plus dynamic) are observed parallel to the magnetic field with consequent reductions in the plasma power and ion fluxes to the limiting surfaces." The primary goal of those studies is to develop the physics and technology of a radiating divertor that will ensure the safe operation of plasma-receiving divertor plates in fusion reactors. For linear confinement systems (different kinds of magnetic mirror traps), the problem of power load to the receiving endplates is less severe. Designs of existing [16–20] or proposed [21–24] mirror confinement systems usually include special end sections where the magnetic field gradually decreases towards the wall. These sections are usually called magnetic expanders. In an expander, the diameter of a magnetic flux tube increases towards the wall, and the power density in the outflowing plasma stream correspondingly decreases. The linear topology of a mirror system allows one to design quite simple expanders with the expansion ratio of up to several hundred and an efficient pumping.

In addition to the task of handling the power flow, expanders perform two other important functions in a mirror trap. Plasma there has a direct electrical contact with conducting receiving endplates. On the one hand, this contributes to plasma stability in the trap due to line-tying effects (see, e.g., [25, 26]). On the other hand, cold electrons from the surface plasma can be accelerated by an ambipolar electric field towards the confinement zone, which usually has a positive potential. The flow of cold electrons from the end can lead to increased longitudinal energy losses and degradation of confinement. To eliminate this effect, expanders with a sufficiently high expansion coefficient of the magnetic field $K \geq (m_i/m_e)^{1/2}$ are used. When this condition is satisfied, the flow of cold electrons into the trap can be suppressed (see, e.g., [27–29]). The transition to the detached mode means a significant change in the role of these factors.
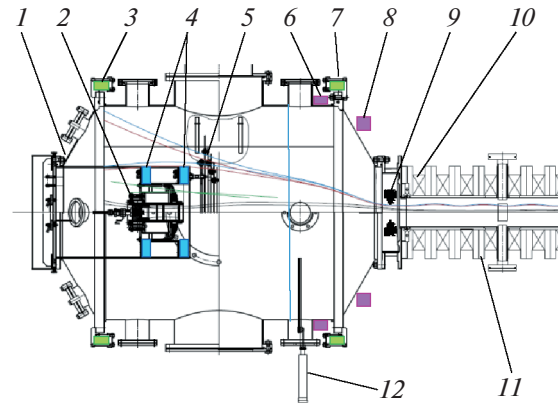
Our interest in studying the detachment mode is related to ensuring the stability and thermal insulation of the plasma in the GOL-NB multiple-mirror trap [18, 30]. The main scenario of the experiment consists in the initial filling of the GOL-NB central trap with
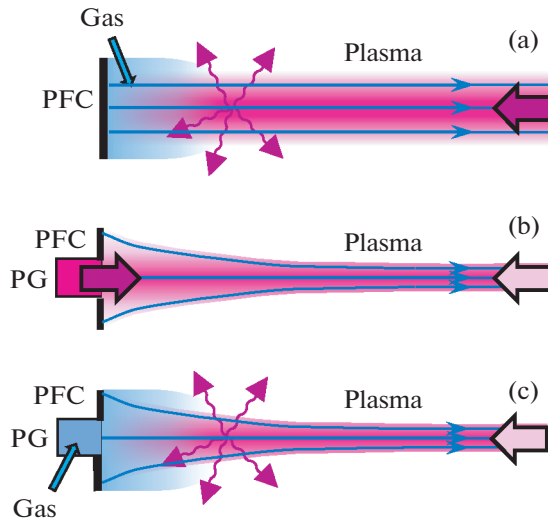
Fig. 1. Layouts of a typical plasma-surface interaction experiment (a) and of two phases of the GOL-NB detachment experiments: the plasma gun operation (b) followed by the detachment (c). PFC is a plasma-facing component, PG is a plasma gun, wavy arrows show a radiating zone, solid lines schematically show magnetic force lines. Plasma and neutral hydrogen differ in color.

Fig. 2. The expander section of GOL-NB with the plasma gun. (*1*) The vacuum vessel, (*2*) the arc plasma gun, (*3*) and (*7*) the expander coils, (*4*) the plasma gun coils, (*5*) the sectioned plasma receiver, (*6*) and (*8*) the expander shaping coils, (*9*) the limiter unit, (*10*) the last coil of the high-field section, (*11*) the high-field section, (*12*) location of the Langmuir probe at $z = 0.54$ m. The axial coordinate z is measured from the plasma gun anode.

a low-temperature starting plasma and its following heating with neutral beams. The starting plasma is created using an arc plasma gun located on the axis in one of the expanders. During the heating stage, the electrical connection between the plasma gun and the plasma must be broken in order to reduce the flow of cold electrons into the confinement region. In this paper, the detachment was provided by an additional gas supply directly into the plasma gun. Figure 1 shows the differences between a typical plasma-surface interaction experiment and our research. Usually, a plasma stream arrives to a plasma-facing surface from an external source like a confinement zone or a dedicated plasma source—see Fig. 1a. Figures 1b and 1c show two successive steps in the reported GOL-NB experiments. Initially, the plasma gun fills the central trap through a strong magnetic mirror, so the magnetic force lines converge in the figure. At the same time, there is also a back plasma flow to the receiving endplates from the strong field side; it is shown by the arrow with less bright color. The resulting plasma footprint on the receiver is larger than the exit aperture of the plasma gun. The second step of the experiment begins with the termination of the current in the plasma gun. In order to achieve the detachment, we varied the duration of hydrogen gas injection into the gun. The back plasma flow from the trap still exists during this step.

In the paper, the details of the experiment and diagnostics are described in Section 2. The plasma properties in the expander section are described in Section 3. Section 4 provides the available data on the stability change in the detached mode. The last section is a discussion and summary.

2. EXPERIMENTAL DEVICE AND DIAGNOSTICS

The GOL-NB facility is the device built for studies of physics of the multiple-mirror confinement [18, 30]. In full configuration, it consists of a central trap of the gasdynamic type with the length of 2.5 m and the magnetic field of $B = 0.3$ T at the center, a 3-m-long sections of the high magnetic field ($B = 4.5$ T) attached to it, and the end magnetic flux expanders. Inside the expanders, there are plasma receiving endplates and the plasma gun with the arc source of hydrogen plasma [31]. The facility design is described in more detail in [32, 33].
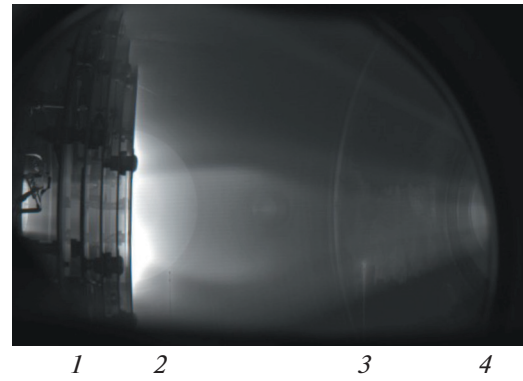
In the paper, we focus on the processes in the input expander near the plasma gun. The layout of this part of GOL-NB is shown in Fig. 2. The vacuum vessel, which houses the plasma gun, the plasma receiving endplates, the input limiter assembly as well as several magnetic coils, has a diameter of 1 meter. The plasma gun usually operates in 0.1–0.2 T magnetic field. Then, the plasma flow propagates towards the high-field section and later, after passing it, fills the central trap. The plasma flow is collisional with the free path length smaller than a typical spatial scale. Most of the plasma from the gun is reflected from the growing magnetic field [34]. The final plasma profile in the input expander looks like a dense central core with a diameter approximately corresponding to the hole in the first electrode of the receiver, surrounded by a less dense halo of reflected plasma, which extends to contact with the limiter [31, 33].
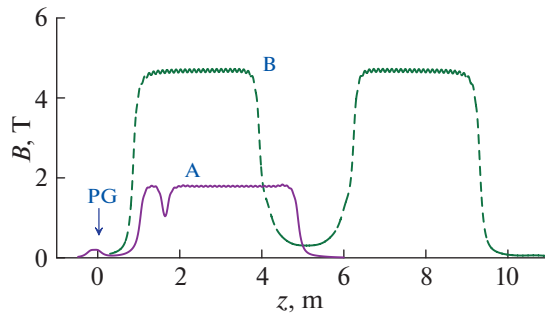
Fig. 3. The axial profiles of the magnetic field in the start (A) and full (B) configurations of GOL-NB. The arrow labeled PG is the plasma gun location.


Fig. 4. The photo of the plasma glow in the gun area taken with a wide-angle lens during an initial cleaning of Langmuir probes by the discharge. Labels are: (*1*) side-on view of five rings of the input plasma receiver with the discharge channel seen in gaps, (*2*) and (*3*) Langmuir probes at $z = 0.20$ and 0.54 m, (*4*) transition to the high-field section. Other objects with a regular geometric shape are elements of the hardware.

The experiments were performed in two different configurations of GOL-NB. The coresponding axial profiles of the magnetic field are shown in Fig. 3. In the next section we will present the results of the detachment studies in the input expander. Those experiments were carried out in the start configuration of GOL-NB (the solid line in Fig. 3) that included both expanders and a single high-field section between them [34]. Due to hardware limitations of the start configuration, the magnetic field in the high-field section was limited to 1.8 T. The second series of experiments was devoted to the effect of detachment on the plasma stability in the central trap. It was carried out in the full design configuration of GOL-NB [32, 33] at 4.5 T in the high-field section (the dashed line in Fig. 3). Configurations A and B differ also in the duration of the discharge current in the plasma gun (2.0 and 2.7 ms, correspondingly).

The main diagnostic tools in our experiments were two movable asymmetric double Langmuir probes. The probes were located at $z = 0.20$ and 0.54 m, see Fig. 4. The probes were connected to a compact battery-fed control and data acquisition module; they operated at a floating potential. We should note two features of probes operation near the plasma gun. The first one is damage to the probe wires by high current in the electron branch of $I{-}V$ characteristics (VAC) in these particular locations. The second one is a deep high-frequency modulation of probe wires currents caused by $E \times B$ rotating current filaments in the discharge; this modulation prevents reliable measurements of VAC. This forced us to simplify the probe heads comparing with the original four-electrode design [35], which is used for plasma properties measurements in other parts of GOL-NB. Only the ion saturation current at a fixed bias and the plasma potential were measured. Therefore, we had no direct data on the dynamics of the plasma temperature. Instead, we used the temperature data from the four-electrode probe placed in a more remote location as the approximate estimate. Further in the text, the measured ion saturation current will be recalculated

into plasma density using the simple model based on [36] under the assumption that at the plasma decay the temperature is 2 eV. In the test experiments discussed in [35], we validated the suitability of the model [36] for measurements of the plasma parameters during the main part of the discharge when the plasma gun was active and for some time after its termination during the plasma decay. The additional gas injection in the experiments with plasma detachment discussed in this paper strongly changes the conditions of the probe operation, including the temperature and the neutral gas density, which are not known. This makes the theoretical model used formally unsuitable. However, for the purpose of this paper we decided to use the same model for all probe signals in order to eliminate the uncertainty associated with the wrong choice of a different theoretical model for poorly known experimental conditions. With this understanding, we will use the plasma density values after the end of the discharge in the plasma gun to visualize the differences in the signals dynamics instead of presenting the raw probe signals. In order to avoid confusion, we will call this quantity the model density.

3. PROPERTIES OF DETACHED PLASMA

In this section, we will present the experimental results obtained in the start configuration of GOL-NB (the solid line in Fig. 3). In this configuration, the plasma stream from the gun passes through the high-field section and dissipates at the exit plasma receiver; no density accumulation in any part of GOL-NB occurs. Figure 5 shows a typical experimental scenario in the standard mode of with the optimized gas supply into the plasma gun. The hydrogen supply starts at $t = -2.0$ ms; it lasts for $t_{gas} = 2.0$ ms (the solid line in
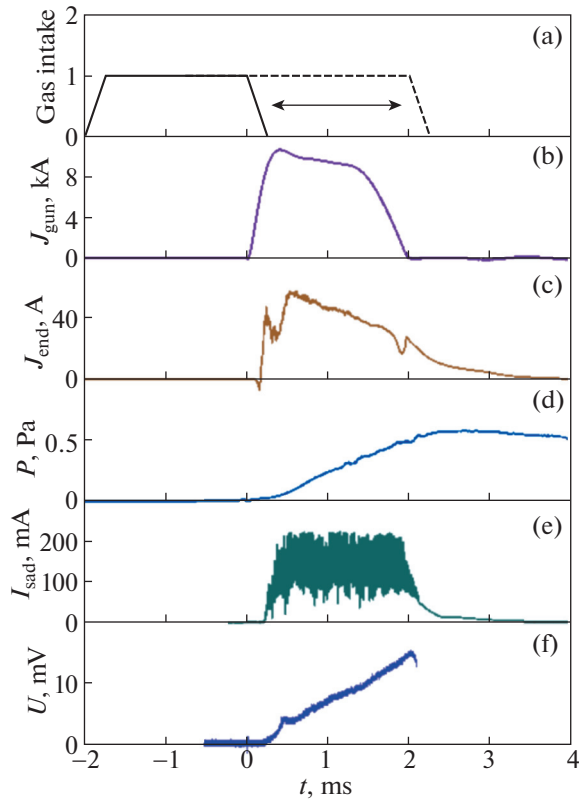
Fig. 5. The experimental scenario and typical waveforms in the experiment NB4333 in the start configuration of GOL-NB (the case A in Fig. 3), top to bottom: the diagram of the gas valve opening time with the standard operation with $t_{gas} = 2$ ms shown by the solid line and an additional gas feed shown by the dashed line, the plasma gun current J_{gun}, the current to the central plasma receiving endplate in the opposite magnetic expander J_{end}, the gas pressure in the plasma gun expander P, the ion saturation current of the Langmuir probe I_{sat}, the photodiode signal in the high-field section U.

Fig. 5a). The duration of the gas supply corresponds to the duration of the discharge current. We use the gas valve [37] with the opening time 0.25 ms. In this case, almost no extra gas stays in the plasma gun volume after the discharge. In the reported experiments on the detachment, we increased the duration of the gas injection t_{gas} using the same gas valve and other related hardware. The dashed line in Fig. 5a schematically shows the increased gas supply.

The shape and duration of the waveform of the discharge current J_{gun} is determined by the parameters of the high-voltage forming line that feeds the gun. It is almost independent on the gas supply parameters, if there is enough gas for the initial breakdown. The current to the central plasma receiving endplate in the opposite magnetic expander J_{end} begins with the time-of-flight delay. The gas pressure in the input expander P, measured at the wall of the vacuum vessel, steadily
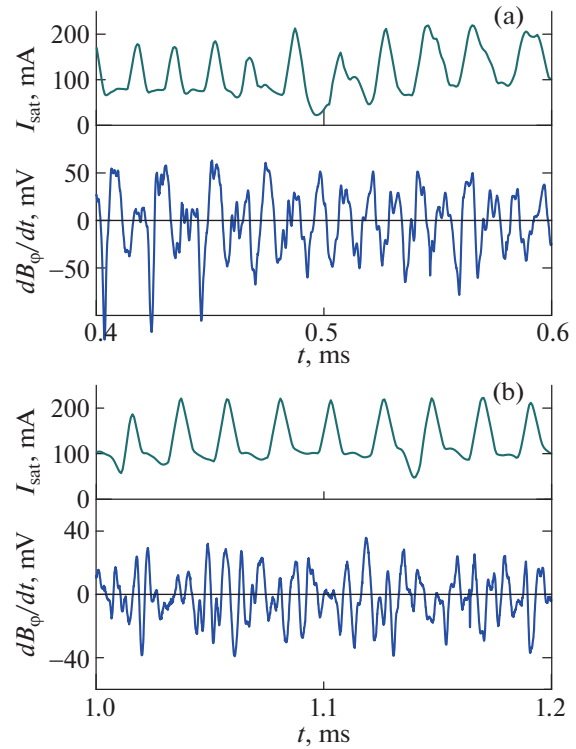
Fig. 6. A high-frequency modulation of the ion saturation current of the Langmuir probe I_{sat} and of the magnetic pickup coil signal dB_φ/dt at $z = 2.68$ m in two fragments of waveforms from the experiment NB4333 (the same as in Fig. 5).
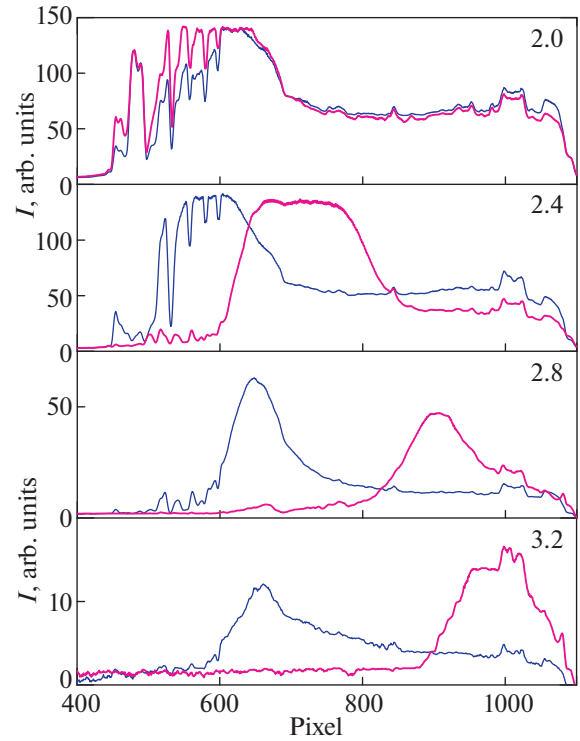
grows during the gun operation. The ion saturation current of the Langmuir probe I_{sat}, demonstrates the mentioned feature of the discharge. It has strong modulation throughout the discharge duration. This means that local plasma parameters in the discharge are modulated. However, with the exception of this modulation, the plasma flow is stable. In [35], we measured the series-averaged plasma parameters for the peaks $T_e \approx 13$ eV and for the background $T_e \approx 7$ eV at $t \approx 1.5$ ms. The modulation of local plasma parameters is most probably caused by a spatial non-uniformity of the current density in the discharge, that causes a spatial non-uniformity of the plasma stream. Due to $E \times B$ rotation of plasma, the probe senses that spatial non-uniformity as the periodical modulation of the measured current. One can note that modulation of the probe signal disappears after termination of the discharge current; the decaying plasma is quieter. The last signal in Fig. 5 is the optical radiation of the plasma column in the high-field section measured with a calorimetric XUV-to-NIR photodiode. Its dynamics is consistent with the steady growth of neutrals pressure at the stable plasma density and temperature.
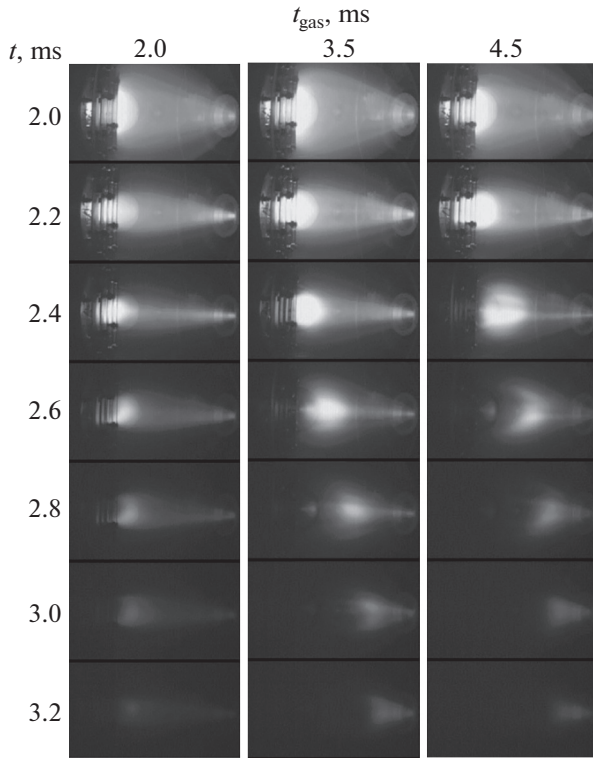
Fig. 7. The dynamics of plasma emission in three discharges with varying gas supply duration t_{gas} at 0.5 MPa initial pressure in the valve. The case with $t_{gas} = 2$ ms is the standard operation mode shown by the solid line in Fig. 5a. The beginning of each frame is shown on the left; the exposure was 7 µs.

Fig. 8. Brightness intensity profiles measured along the magnetic axis for selected frames from Fig. 7. Thick lines correspond to the detached mode with $t_{gas} = 3.5$ ms (the central column in Fig. 7); thin lines correspond to the standard mode with $t_{gas} = 2$ ms. The beginning of each frame is shown by labels.

Figure 6 shows the comparison of the fast modulation of signals from the Langmuir probe and from a magnetic pickup coil that measured dB_φ/dt and was located near the wall at $z = 2.68$ m in the high-field section. The important difference in the interpretation of this pair of signals is that the probe provides localized measurements of the plasma parameters and the coil detects variations of the azimuthal magnetic field generated by axial currents, which has some spatial structure in the plasma column. One can see that the lowest-frequency modulation of the ion saturation current is not visible in the magnetic signal that is determined by time-dependent higher-frequency processes, which are most probably localized in the periphery. We can conclude from Fig. 6 that fluctuations measured by the magnetic probe are caused by processes in plasma and not by the initial modulation of the plasma stream.

Figure 7 shows three sets of frames from high-speed videos made in the standard mode (the left column) and in the detachment mode (the central and right columns). The field of view is similar to that shown in Fig. 4. In all three cases, the discharge current in the gun terminated in $t = 2.0$ ms. The plasma is attached to the receiver plates in the standard mode.

The middle column corresponds to the case when the gas supply terminates at $t = 1.5$ ms during the gun operation. One can see the decaying discharge channel in the gaps between the receiver electrodes at $t = 2.4$ ms. Then, the bright radiating zone detaches from the endplates; the radiating plasma is sustained by the return plasma flow from the high-field section for some time. The right column shows the case with even longer gas supply and earlier plasma detachment. In the detached mode, a dark zone between the endplates and the radiating plasma is clearly visible. Later in this section of the text we will discuss the plasma properties for two modes with $t_{gas} = 2$ and 3.5 ms.

The brightness profiles along the magnetic axis for the standard and detached operation modes are compared in Fig. 8 for four pairs of frames from Fig. 7 taken at $t_{gas} = 2$ and 3.5 ms. Due to the wide-angle lens, the x coordinate along the axis is non-linear; therefore, we present the column numbers of the CCD camera as the x coordinate. The light is collected along the lines of sight that have different angles to the axis. We should also note that sharp signal changes are caused by changes in the reflectivity of the opposite wall of the vacuum chamber and by the receiving endplates at $x < 600$. The dark frames were subtracted
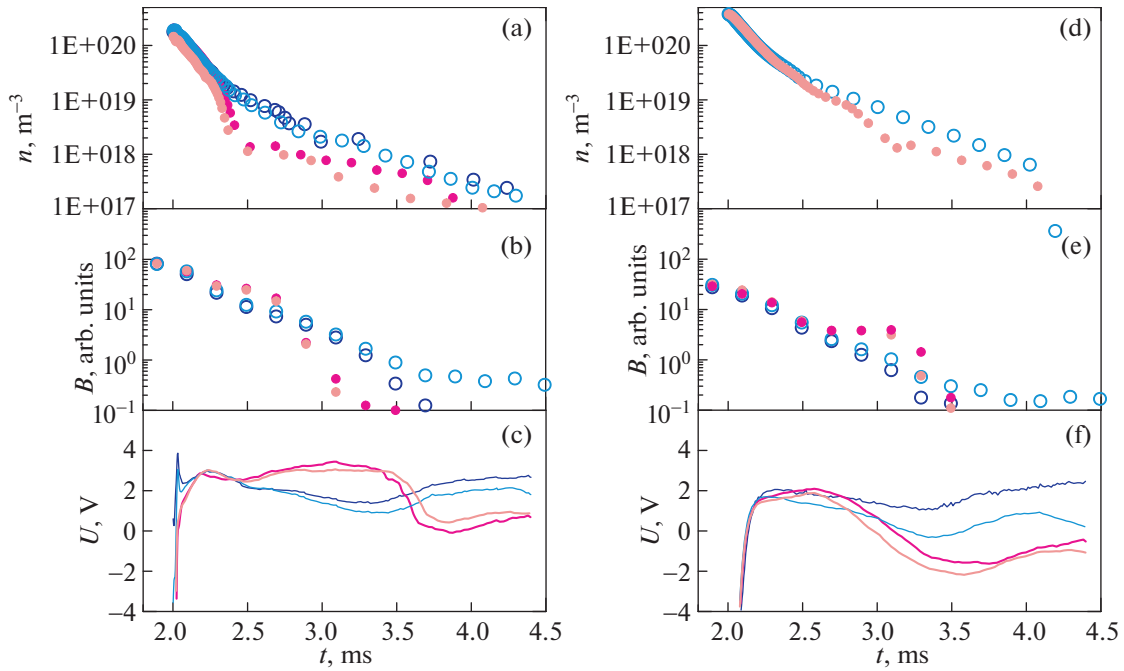
Fig. 9. The dynamics of plasma parameters in the detached and normal operation modes measured at $z = 0.20$ m (left) and 0.54 m (right). Top to bottom: the model density from the probe measurements n, the plasma brightness at the probe location B, and the plasma potential U. Solid dots and thick lines correspond to the detached mode with $t_{gas} = 3.5$ ms (the central column in Fig. 7); open circles and thin lines correspond to the standard mode with $t_{gas} = 2$ ms. The experimental data obtained on different days differ in the color intensity.

from the images. After that, values of four adjacent CCD rows were averaged in order to decrease the digitization noise. No other image processing was performed.

At the moment of the termination of the plasma gun current at $t = 2.0$ ms the brightness profiles for both modes are almost identical at $x > 600$, i.e., in the free space after the receiving endplates. At the same time, one can see lower brightness in the discharge channel at $x < 600$ in the standard operation mode. That is naturally explained by the pre-programmed hydrogen depletion at the time. In the detachment mode, the continuing gas feed provides higher density inside the gun during the current termination. The detachment of the bright plasmoid from the endplates occurs in $t \approx 2.4$ ms at $t_{gas} = 3.5$ ms. After that, the detached plasma moves towards the high-field magnetic mirror. One can see that two modes differ in brightness in about an order of magnitude near the endplate.

The high-speed videos show the significant decrease in plasma brightness near the wall in the detached mode. Here, the plasma emits mostly hydrogen lines in the visible spectrum. At low temperatures, both the electron-impact excitation and the recombination contribute to the radiating power. A possible explanation of the observed decrease in local brightness could be a decrease in the local plasma density when the additionally supplied gas arrives to the obser-

vation point. In a weakly ionized dark region, neutrals provide the pressure balance. However, the probe measurements reveal a more complicated evolution of plasma properties. Figure 9 shows the dynamics of plasma parameters at two locations of the Langmuir probes at $z = 0.20$ and 0.54 m in two modes, which correspond to the left and central columns in Fig. 7. In this figure, we have shown the data obtained on different experimental days using color intensity variations in order to demonstrate the reproducibility. Just like in the video images, these graphs show the arrival of additional hydrogen at the observation point.

Before the termination of the discharge current, which reaches $J_{gun} \approx 10$ kA, the plasma has a large negative potential that is determined by a good electrical connection to the plasma gun cathode. Following that, the plasma in the expander section acquires a natural positive potential of the order of the electron temperature that is about 2 eV in the decaying plasma (panels (c) and (f) in Fig. 9). In the standard mode, that positive potential lasts all the time of plasma decay. We should note that the termination of the current in the power supply circuit of the plasma gun does not mean the instantaneous termination of all currents in the plasma; some loop-like current structures may exist for some time. Residual currents provide the leakage of electric charge to the electrodes and the observed variations of the plasma potential. In the detached mode, the arrival of the dense gas to the

observation point at $z = 0.54$ m (Fig. 9c) results in the reverse change of the polarity to negative. At a closer coordinate $z = 0.20$ m, a similar effect of the gas on the potential begins at a later moment $t \approx 3.4$ ms (Fig. 9f). However, before that we observe some increase in the positive potential comparing with the standard mode.

The high-speed video correlated in general with measurements of the potential (panels (b) and (e) in Fig. 9). All significant changes in the dynamics of the potential have corresponding changes in the dynamics of brightness, with a caveat regarding the light collection along the inclined line of view of the video camera. At first, the brightness increases when the gas comes to the observation point. Then the density of exciting electrons decreases and a decrease in brightness is observed.

The Langmuir probe data is shown in panels (a) and (d) in Fig. 9. We observed a decrease in the ion saturation current by an order of magnitude when at $t \approx 2.3$ ms the gas entered the probe location at $z = 0.20$ m (Fig. 9a, the measured current was recalculated to the model density). Shortly before this, the energy flow from the gun was blocked by the dense gas. The difference between the standard and the detached mode is maximum at $t \approx 2.5$ ms, and then there is some probe signal recovery. At the second probe measurements location $z = 0.54$ m, similar processes occur with a time delay.

Comparison of waveforms in Fig. 9 demonstrates that the change in plasma brightness is more pronounced than the change in ion saturation current (two vs. one order of magnitude, correspondingly). This can be explained by the assumption that electrons from the distribution tail, which have sufficient energy to excite a hydrogen atom at the Langmuir probe location, have already been previously slowed down in the radiating detached plasma.

The reason for the observed partial recovery of the probe signal after the significant initial drop at $t \approx 2.5$ ms in Fig. 9a is not clear at the moment. The system has no external power applied to plasma during this period. The usual theory of Langmuir probes approximates the ion saturation current as follows

$$I_{sat} \approx \alpha n e A \sqrt{T_e/M}, \tag{1}$$

where $\alpha \approx 0.6$ (see, e.g., [38]), A is the probe area, n, e, T_e and M are number density, elementary charge, electron temperature and ion mass, correspondingly. The set of video frames in Fig, 7 shows that the detached radiating plasma still moves forward during this time. Consequently, a simple growth of local plasma parameters due to energy flux from the main plasma column is unlikely; the absence of a simultaneous increase in local brightness does not support such assumption. Probably, here we met the instrumental feature of the probe operation at varying conditions. A Langmuir probe collects the ion saturation current from some plasma sheath, the properties of which vary depending on local plasma and neutral population parameters. The plasma sheath properties are hidden in the α parameter in (1). Supposedly, a change in the sheath parameters due to the fast increase of the gas density can lead to the observed effect.

The Langmuir probe measurements show that some significant population of charged particles exists even behind the radiating detached plasma. The electrical conductivity in this region is determined by collisions of electrons with neutral particles whose density exceeds the plasma density. However, some longitudinal electrical conductivity persists throughout the observation time. The existing theory of plasma MHD stabilization by the line-tying effect suggests that a dense enough plasma exists near the receiving end walls. The line-tying does not provide the true stabilization; it reduces the instability growth rate instead. The stabilizing plasma density n_s should be high enough comparing with the confined plasma density n_c [25, 26]:

$$\frac{n_s}{n_c} > \frac{\Lambda m^2 c_s}{\omega_{ci}^2} \frac{v_i}{r_c^2}, \tag{2}$$

where $\Lambda \geq 10$ is the required reduction of the instability growth rate, m is the azimuthal mode number, r_c is the radius of the confined plasma, and other designations are standard. In the standard mode of the plasma gun operation, the gradual loss of the stabilizing effect of the end plasma occurs as a result of a decrease in its density. In the detachment mode, the loss of stabilizing qualities can occur faster due to the deterioration of longitudinal conductivity because of collisions with neutral particles.

4. MAGNETIC ACTIVITY IN THE CENTRAL TRAP OF GOL-NB

A limited series of experiments with the detached mode of the plasma gun operation was carried out in the full design configuration of GOL-NB. The configuration differed from the one discussed in previous section by the presence of the central trap and the second solenoidal section after it, as well as an increased magnetic field in the solenoids to 4.5 T—see line B in Fig. 3. In general, the operating regime of the plasma gun was close to that shown in Fig. 5, except for the increased duration of the discharge current from 2.0 to 2.7 ms and a similar increase in the duration of the gas supply in the standard mode. The remaining parameters of the experiment were the same as discussed in the previous section. No neutral beams injection was used in the central trap. The magnetic activity of the plasma was studied using two sensors. The first one measured all three components of the magnetic field near the middle plane of the central trap at $z = 5.00$ m. The second sensor measured the azimuthal component of the magnetic field in the solenoidal section at $z = 2.35$ m. Both sensors have multi-turn pickup coils
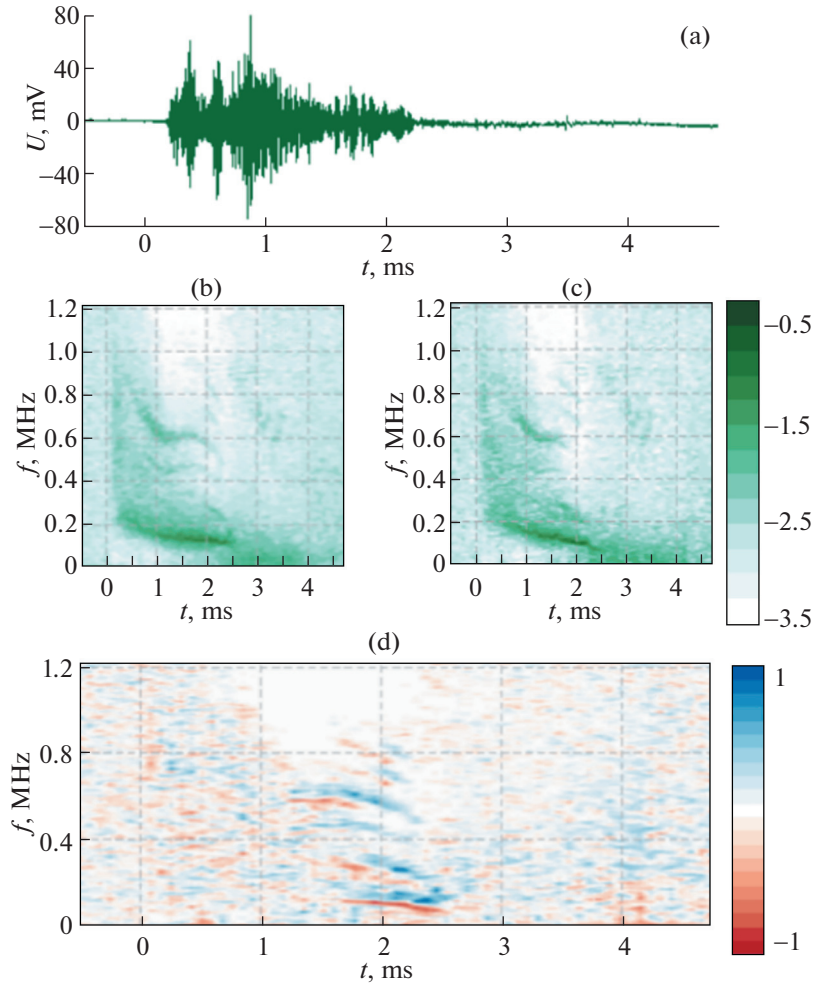
Fig. 10. Magnetic fluctuations spectra at $z = 5.00$ m. (a) is a typical raw signal of the azimuthal coil, (b) is the decimal logarithm of the normalized Fourier spectrogram in the standard operation mode with $t_{gas} = 2.8$ ms, (c) is the same in the detachment mode with $t_{gas} = 5.8$ ms, (d) is the difference between (b) and (c). Here, the difference of 1 corresponds to the difference in the amplitudes of normalized Fourier harmonics by 10 times; blue color—amplitude is higher in the standard mode, red color—amplitude is higher in the detached mode.

protected by grounded electrostatic screens made of 20-μm stainless foil.

Figure 10 shows the data from the azimuthal coil located at $z = 5.00$ m in the central trap. The data from the radial and axial coils look similar, but contain more digital noise due to smaller signal amplitudes. Part (a) of the figure shows a typical signal dB_φ/dt measured in the standard mode. It starts when plasma arrives to the central trap and has large amplitude until the discharge current in the plasma gun begins to decrease significantly. During this high-current part of the discharge, the magnetic signal is modulated similar to that shown in Fig. 6. After that, the signal decreases significantly in amplitude, but it is still suitable for Fourier analysis.

Parts (b) and (c) of Fig. 10 show the Fourier spectra of the dB_φ/dt signals in the standard and detached modes. For the purposes of this article, we have chosen a special form for presenting the results of the Fourier analysis, which allows us to plot the spectral composition of the signal with equal quality during the main phase of the discharge and after its termination. The complete data set of 32 K measurements was divided into 63 intervals of 1024 points, sequentially shifted in time by 512 points. Then, the Fourier analysis was performed for each data set with the Hann weighing function, which has the form

$$\omega(n) = \sin^2\left(\frac{\pi n}{N}\right), \quad 0 \le n \le N, \tag{3}$$

where $N = 1023$ in our case. After that, the Fourier spectra are normalized as follows

$$\hat{f}_{n,norm} = \hat{f}_n / \sum_{k=1}^{N/2} \hat{f}_k, \tag{4}$$

where $\hat{f}_n$ is the amplitude of nth Fourier harmonics. Then, a decimal logarithm of the normalized harmonics was plotted in Fig. 10. With this definition, the case of $\hat{f}_{n,\text{norm}} = 1$ corresponds to a single frequency harmonic in the signal, regardless of its actual amplitude.

Part (d) of Fig. 10 shows the difference in the magnetic fluctuations in two operating modes. One can see that fluctuations of the highest physical amplitude with frequencies in the ranges of 0.1−0.2 and 0.6−0.7 MHz, associated with the peculiarities of the plasma gun operation, practically disappear in the difference spectrogram. The most pronounced feature of the difference spectrum is the fluctuation modes with frequencies in the range from 0.1 to 0.9 MHz, which occur at the phase of decreasing discharge current in the gun. The frequency of these modes gradually decreases with time, and there is a transition of the maximum amplitude to the modes with the lowest frequency. These modes correspond, most likely, to interchange-like perturbations with different azimuthal mode numbers, which rotate together with the plasma due to $E \times B$ drift. Such identification is based on the following. The plasma imaging with a frame duration of 7 μs shows a typical pattern of brighter and darker stripes aligned along the magnetic field, which begin to form at the end of the discharge current. At longer frame durations, the pattern is blurred due to plasma rotation. The radial electric field is specially created by a system of biased limiters and end plasma receivers (see [32, 33] for details); it was directly measured in [34] in the same configuration and operation regime as that presented in Section 3. In the detachment mode, the discussed magnetic fluctuations occur earlier and have a lower frequency, which may be due to a worse translation of the electric potential along the magnetic field with the additional gas supply at the end of the discharge.

During the main part of the discharge in the plasma gun, a gradual accumulation of plasma occurs in the central trap, see Fig. 6 in [32]. The density growth stops approximately at the same time when the signs of interchanges appear in the magnetic signals. The line-tying stabilization condition (2) is violated at one point with a gradual decrease in plasma density in the standard mode. In the detached mode, plasma destabilization occurs earlier due to worse electrical conductivity of the expander plasma.

5. SUMMARY

Two series of experiments with additional hydrogen injection into the plasma gun were carried out at different configurations of the GOL-NB magnetic mirror trap. Near the plasma gun, we observed the appearance of a radiating plasma formation detached from the surface, which visually corresponds to that in radiating divertors in tokamaks. Direct in situ probe measurements showed that changes in the dynamics of the ion saturation current of the probe are less than changes in the visible brightness of this area when switching to the detachment mode. In both the standard and the detached modes, decaying plasma existed near the receiving electrodes for the entire observation time after the termination of the discharge current.

Measurements of the magnetic fluctuations spectrum in the central trap of GOL-NB have shown that in the detachment mode, some structures in the Fourier spectrogram of magnetic fluctuations with frequencies in the range of 0.1−0.9 MHz manifest earlier than in the standard mode and have lower frequencies. We associate these structures in magnetic fluctuations with the onset of interchange modes due to the loss of plasma stabilization by the line-tying to the conducting ends. On the whole, the observed plasma behavior in the detached mode confirmed our understanding of the line-tying effect as the main factor stabilizing the plasma core in the initial phase of density accumulation in the central trap. In the GOL-NB physical project, it is assumed that the vortex confinement technique [38] will be used to stabilize the neutral-beam heated plasma during the main phase of the experiment, see details in [18, 39].

CONFLICT OF INTEREST

The authors of this work declare that they have no conflicts of interest.

REFERENCES

1. J. Boedo, A. G. McLean, D. L. Rudakov, and J. G. Watkins, Plasma Phys. Controlled Fusion **60**, 044008 (2018).
   https://doi.org/10.1088/1361-6587/aaa2ec

2. M. Cavedon, B. Kurzan, M. Bernert, D. Brida, R. Dux, M. Griener, S. Henderson, E. Huett, T. Nishizawa, T. Lunt, O. Pan, U. Stroth, M. Wischmeier, E. Wolfrum, and the ASDEX Upgrade Team, Nucl. Fusion **62**, 066027 (2022).
   https://doi.org/10.1088/1741-4326/ac6071

3. Y. Feng, M. Jakubowski, R. König, M. Krychowiak, M. Otte, F. Reimold, D. Reiter, O. Schmitz, D. Zhang, C. D. Beidler, C. Biedermann, S. Bozhenkov, K. J. Brunner, A. Dinklage, P. Drewelow, et al., Nucl. Fusion **61**, 086012 (2021).
   https://doi.org/10.1088/1741-4326/ac0772

4. X. Guo, H. Tanaka, S. Kajita, N. Ohno, S. Hattori, and K. Sawada, Plasma Fusion Res. **17**, 2402027 (2022).
   https://doi.org/10.1585/pfr.17.2402027

5. M. S. Islam, Y. Nakashima, A. Hatayama, H. Matsuura, K. Ichimura, T. Iijima, T. Yokodo, K. Nojiri, A. Terakado, M. M. Islam, T. Yoshimoto, S. Yamashita, T. Hara, M. Yoshikawa, N. Ezumi, et al., Plasma Fusion Res. **14**, 2402016 (2019).
https://doi.org/10.1585/pfr.14.2402016

6. K. Ješko, Y. Marandet, H. Bufferand, J. P. Gunn, H. J. van der Meiden, and G. Ciraolo, Plasma Phys. Controlled Fusion **60**, 125009 (2018).
https://doi.org/10.1088/1361-6587/aae80d

7. I. J. Kang, M.-K. Bae, I. S. Park, H.-J. Woo, T. Lho, J.-S. Ahn, D.-H. Chang, S.-G. Cho, G.-S. Choi, H.-G. Choi, Y.-S. Choi, B.-H. Chung, T. H. Chung, J.-J. Do, B.-C. Goo, et al., J. Korean Phys. Soc. **80,** 717 (2022).
https://doi.org/10.1007/s40042-022-00397-y

8. A. W. Leonard, Plasma Phys. Controlled Fusion **60**, 044001 (2018).
https://doi.org/10.1088/1361-6587/aaa7a9

9. K. Mukai, S. Masuzaki, Y. Hayashi, T. Oishi, C. Suzuki, M. Kobayashi, T. Tokuzawa, H. Tanaka, K. Tanaka, T. Kinoshita, H. Sakai, and B. J. Peterson, Nucl. Fusion **61**, 126018 (2021).
https://doi.org/10.1088/1741-4326/ac2bbc

10. R. Perillo, R. Chandra, G. R. A. Akkermans, I. G. J. Classen, S. Q. Korving, and Magnum-PSI Team, Phys. Plasmas **26**, 102502 (2019).
https://doi.org/10.1063/1.5120180

11. R. A. Pitts, X. Bonnin, F. Escourbiac, H. Frerichs, J. P. Gunn, T. Hirai, A. S. Kukushkin, E. Kaveeva, M. A. Miller, D. Moulton, V. Rozhansky, I. Senichenkov, E. Sytova, O. Schmitz P. C. Stangeby, et al., Nucl. Mater. Energy **20**, 100696 (2019).
https://doi.org/10.1016/j.nme.2019.100696

12. A. A. Shoshin, A. S. Arakcheev, A. V. Arzhannikov, A. V. Burdakov, I. A. Ivanov, A. A. Kasatov, K. N. Kuklin, S. V. Polosatkin, V. V. Postupaev, S. L. Sinitsky, A. A. Vasilyev, and L. N. Vyacheslavov, Fusion Eng. Design **114**, 157 (2017).
https://doi.org/10.1016/j.fusengdes.2016.12.019

13. V. A. Soukhanovskii, S. L. Allen, M. E. Fenstermacher, C. J. Lasnier, M. A. Makowski, A. G. McLean, W. H. Meyer, D. D. Ryutov, E. Kolemen, R. J. Groebner, A. W. Hyatt, A. W. Leonard, T. H. Osborne, T. W. Petrie, and J. Watkins, Nucl. Fusion **58**, 036018 (2018).
https://doi.org/10.1088/1741-4326/aaa6de

14. L. Wang, H. Q. Wang, D. Eldon, Q. P. Yuan, S. Ding, K. D. Li, A. M. Garofalo, X. Z. Gong, G. S. Xu, H. Y. Guo, K. Wu, L. Y. Meng, J. C. Xu, J. B. Liu, M. W. Chen, et al., Nucl. Fusion **62**, 076002 (2022).
https://doi.org/10.1088/1741-4326/ac4774

15. G. F. Matthews, J. Nucl. Mater. **220−222**, 104 (1995).
https://doi.org/10.1016/0022-3115(94)00450-1

16. H. Gota, M. W. Binderbauer, T. Tajima, A. Smirnov, S. Putvinski, M. Tuszewski, S. A. Dettrick, D. K. Gupta, S. Korepanov, R. M. Magee, J. Park, T. Roche, J. A. Romero, E. Trask, X. Yang, P. Yushmanov, K. Zhai, T. DeHaas, et al., Nucl. Fusion **61**, 106039 (2021).
https://doi.org/10.1088/1741-4326/ac2521

17. Q. Li, G. Zhu, B. Ren, J. Ying, Z. Yang, and X. Sun, Plasma Sci. Technol. **25**, 025102 (2023).
https://doi.org/10.1088/2058-6272/ac8e45

18. V. V. Postupaev, V. I. Batkin, A. D. Beklemishev, A. V. Burdakov, V. S. Burmasov, I. S. Chernoshtanov, A. I. Gorbovsky, I. A. Ivanov, K. N. Kuklin, K. I. Mekler, A. F. Rovenskikh, E. N. Sidorov, and D. V. Yurov, Nucl. Fusion **57**, 036012 (2017).
https://doi.org/10.1088/1741-4326/57/3/036012

19. A. V. Sudnikov, A. D. Beklemishev, V. V. Postupaev, A. V. Burdakov, I. A. Ivanov, N. G. Vasilyeva, K. N. Kuklin, and E. N. Sidorov, Fusion Eng. Design **122**, 86 (2017).
https://doi.org/10.1016/j.fusengdes.2017.09.005

20. D. V. Yakovlev, A. G. Shalashov, E. D. Gospodchikov, V. V. Maximov, V. V. Prikhodko, V. Ya. Savkin, E. I. Soldatkina, A. L. Solomakhin, and P. A. Bagryansky, Nucl. Fusion **58**, 094001 (2018).
https://doi.org/10.1088/1741-4326/aacb88

21. D. I. Skovorodin, I. S. Chernoshtanov, V. Kh. Amirov, V. T. Astrelin, P. A. Bagryanskii, A. D. Beklemishev, A. V. Burdakov, A. I. Gorbovskii, I. A. Kotel'nikov, E. M. Magommedov, S. V. Polosatkin, V. V. Postupaev, V. V. Prikhod'ko, V. Ya. Savkin, E. I. Soldatkina, et al., Plasma Phys. Rep. **49**, 1039 (2023).
https://doi.org/10.1134/S1063780X23600986

22. P. A. Bagryansky, A. D. Beklemishev, and V. V. Postupaev, J. Fusion Energy **38**, 162 (2019).
https://doi.org/10.1007/s10894-018-0174-1

23. P. A. Bagryansky, Z. Chen, I. A. Kotelnikov, D. V. Yakovlev, V. V. Prikhodko, Q. Zeng, Y. Bai, J. Yu, A. A. Ivanov, and Y. Wu, Nucl. Fusion **60**, 036005 (2020).
https://doi.org/10.1088/1741-4326/ab668d

24. J. Egedal, D. Endrizzi, C. B. Forest, and T. K. Fowler, Nucl. Fusion **62**, 126053 (2022).
https://doi.org/10.1088/1741-4326/ac99ec

25. R. Prater, Phys. Fluids **17**, 193 (1974).
https://doi.org/10.1063/1.1694587

26. A. W. Molvik, R. A. Breun, S. N. Golovato, N. Hershkowitz, B. McVey, R. S. Post, D. Smatlak, and L. Yujiri, Phys. Fluids **27**, 2711 (1984).
https://doi.org/10.1063/1.864575

27. I. K. Konkashbaev, I. S. Landman, and F. R. Ulinich, Sov. Phys.−JETP **47**, 501 (1978).

28. I. S. Abramov, E. D. Gospodchikov, R. A. Shaposhnikov, and A. G. Shalashov, Nucl. Fusion **59**, 106004 (2019).
https://doi.org/10.1088/1741-4326/ab2ef8

29. D. I. Skovorodin, Phys. Plasmas **26**, 012503 (2019).
https://doi.org/10.1063/1.5043072

30. V. V. Postupaev, A. V. Burdakov, and A. A. Ivanov, Fusion Sci. Technol. **68**, 92 (2015).
https://doi.org/10.13182/FST14-846

31. I. A. Ivanov, V. I. Batkin, A. V. Burdakov, K. N. Kuklin, K. I. Mekler, V. V. Postupaev, A. F. Rovenskikh, and E. N. Sidorov, Plasma Phys. Rep. **47**, 938 (2021).
https://doi.org/10.1134/S1063780X21090026

32. V. V. Postupaev, V. I. Batkin, A. V. Burdakov, V. S. Bur-masov, I. A. Ivanov, K. N. Kuklin, Yu. A. Lykova, N. A. Melnikov, K. I. Mekler, A. V. Nikishin, S. V. Po-losatkin, A. F. Rovenskikh, E. N. Sidorov, and D. I. Skovorodin, Nucl. Fusion **62**, 086003 (2022). https://doi.org/10.1088/1741-4326/ac69fa

33. I. A. Ivanov, P. A. Polozova, V. I. Batkin, K. N. Kuklin, V. V. Kurkuchekov, N. A. Melnikov, S. V. Polosatkin, V. V. Postupaev, A. F. Rovenskikh, E. N. Sidorov, and D. I. Skovorodin, Plasma Phys. Rep. **49**, 1251 (2023). https://doi.org/10.1134/S1063780X23601591

34. V. V. Postupaev, V. I. Batkin, A. V. Burdakov, V. S. Bur-masov, I. A. Ivanov, K. N. Kuklin, K. I. Mekler, A. F. Rovenskikh, and E. N. Sidorov, Plasma Phys. Controlled Fusion **62**, 025008 (2020). https://doi.org/10.1088/1361-6587/ab53c2

35. E. N. Sidorov, V. I. Batkin, A. V. Burdakov, I. A. Iva-nov, K. N. Kuklin, K. I. Mekler, A. V. Nikishin, V. V. Postupaev, and A. F. Rovenskikh, J. Instrum. **16**, T11006 (2021). https://doi.org/10.1088/1748-0221/16/11/T11006

36. J. G. Laframboise, PhD Thesis (Institute for Aerospace Studies, University of Toronto, Toronto, 1966).

37. G. E. Derevyankin, V. G. Dudnikov, and P. A. Zhurav-lev, Prib. Tekh. Exp., No. 5, 168 (1975).

38. F. F. Chen, in *Proceedings of the 2003 IEEE International Conference on Plasma Science* (Jeju, 2003), p. 20. https://www.seas.ucla.edu/~ff-chen/Publs/Chen210R.pdf.

39. A. D. Beklemishev, P. A. Bagryansky, M. S. Chaschin, and E. I. Soldatkina, Fusion Sci. Technol. **57**, 351 (2010). https://doi.org/10.13182/FST10-A9497

Publisher's Note. Pleiades Publishing remains neutral with regard to jurisdictional claims in published maps and institutional affiliations.